Unbroken Metal Rim MIMO Antenna Utilizing Antenna Clusters

Rasmus Luomaniemi, *Student Member, IEEE*, Jari-Matti Hannula, *Member, IEEE*, Riku Kormilainen, Anu Lehtovuori, and Ville Viikari, *Senior Member, IEEE*

***Abstract*—This letter presents an antenna system for mobile devices with an unbroken metal rim. By utilizing the characteristic mode analysis for the unbroken metal rim, efficient multiple-input–multiple-output operation can be achieved. The design is based on an antenna cluster technique that uses several coupled elements that are used to efficiently excite the modes of the rim. Nonresonant antenna elements and matching networks are used to couple to the metal rim. The design has small ground clearance of 5 mm and height of only 4 mm, and can operate in wide bandwidths both in 700–960 MHz low band and 1.56–4 GHz high band. Measurement results confirm that competent performance is achieved.**

***Index Terms*—Characteristic modes, mobile antennas, multiple-input–multiple-output (MIMO), unbroken metal rim.**

I. Introduction

In THE last few years, the evolution of smart phones has been driven mainly by two factors. First, the appearance of the device must be attractive to the users. Therefore, the devices are equipped with larger and larger screens and they are metal-framed. Second, the demand for higher data rates requires the use of multiple-input–multiple-output (MIMO) techniques and new frequency ranges such as the 3.5 GHz band.

It is well known that metal rim significantly affects the performance of traditionally used internal antennas [1]. In most published designs, the metal rim is cut into several pieces that act as antennas; see, e.g., [2]–[6]. However, cuts in the metal frame are demanding to manufacture, they lower the physical robustness, and hinder the visual appearance of the device. When the metal rim is kept completely intact, the antenna design is typically more difficult. Many of the unbroken metal rim antennas combine the operation of several different current loops in the metal rim with the ground plane structure for wideband operation [7]–[15]. However, the published designs have several weaknesses. They are lacking the operation at the 700 MHz and the 3.5 GHz bands, and most of them require large ground clearances unsuitable for the current trends in smart phones. Only a few of them are capable of MIMO operation both in the low and high band [12], [14]. Therefore, new ways of utilizing the unbroken metal rim as an antenna are needed.

A major problem with the unbroken metal rim is the high coupling between the antennas if they are, e.g., placed to the opposite short edges of the device, which is often the case for MIMO antennas. In this letter, we utilize for the first time the characteristic mode analysis (CMA) combined with the antenna cluster technique [16], [17]. With the antenna cluster method, multiple antenna elements are used collaboratively to benefit from normally harmful high mutual coupling between the elements, and with CMA, antenna clusters with low correlation can be designed. Thus, good MIMO performance in a device with an unbroken metal rim and a small ground clearance can be achieved. In previous cluster designs, the antenna elements have been self-resonant and an unbroken metal rim has not been used. In this letter, for the first time, we combine the antenna cluster technique with nonresonant antenna elements and matching circuits. By using the clusters formed from several coupled elements fed with complex weighted signals, the modes of the metal rim can be excited more efficiently than with traditional techniques. The design procedure is described, and both the simulation and measurement results are presented. The results show that good performance is achieved despite the challenging environment of a small ground clearance and an unbroken metal rim.

II. Theoretical Background

A. Characteristic Mode Analysis

CMA is a computational tool used to study the electromagnetic properties of an antenna structure without any specific excitations [18]. The resulting current distributions can be used for determining the feed locations for the antenna elements. The orthogonal modes can be excited separately with multiple exciters for good MIMO performance as is done, e.g., in [10], [19], [20], and in this letter, or multiple modes can be combined by modifying the structure to be excited with a single exciter for increased bandwidth [8], [15]. Below 1 GHz, there is only one dominant mode for a regular ground plane of a phone-sized device, which is the $\lambda/2$ dipole-type resonance along the longer dimension. This makes implementing MIMO antennas with low correlation difficult [21]. However, when an unbroken metal rim is combined with the ground plane, new modes with resonant frequencies below the ground plane mode are created.

The Integral Equation Solver of CST Microwave Studio is used to study the characteristic modes of an unbroken metal

Manuscript received February 26, 2019; accepted March 19, 2019. Date of publication April 16, 2019; date of current version May 31, 2019. This work was conducted within the 5G TRx project supported in part by Business Finland, in part by Nokia Bell Labs, in part by Huawei Technologies Finland, in part by RF360, in part by Pulse Electronics Finland, and in part by Sasken Finland. *(Corresponding author: Rasmus Luomaniemi.)*

The authors are with the Department of Electronics and Nanoengineering, Aalto University School of Electrical Engineering, Espoo 00076, Finland (e-mail: rasmus.luomaniemi@aalto.fi; jari-matti.hannula@aalto.fi; riku.kormilainen@aalto.fi; anu.lehtovuori@aalto.fi; ville.viikari@aalto.fi).

Digital Object Identifier 10.1109/LAWP.2019.2906993

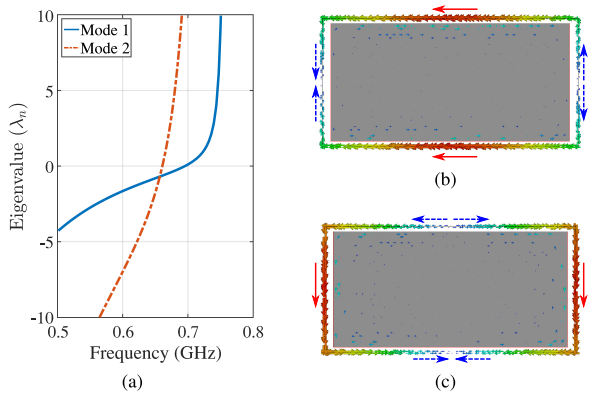

Fig. 1. (a) Eigenvalues and characteristic current distributions of the first two modes for an unbroken metal rim and a ground plane (b) mode 1 and (c) mode 2. Current maxima are shown with solid arrows, and minima with dashed arrows.

rim structure. The size of the ground plane is 140 $\times$ 69 mm^2 and the size of the metal rim is 150 $\times$ 75 $\times$ 4 mm^3, i.e., the ground clearances are 5 mm on the short edges and 3 mm on the long edges. The results for the first two resonating modes are shown in Fig. 1. The eigenvalues are shown in Fig. 1(a), and the corresponding current distributions at the resonance frequencies in Fig. 1(b) and (c).

The metal rim has two modes at the low-band frequencies that can be used to achieve good MIMO performance. These orthogonal modes can theoretically be excited separately by placing, e.g., capacitive coupling elements near the current minima of each mode [19]. The slope of the eigenvalue at resonance ($\lambda_n = 0$) describes the potential of the mode to achieve wideband operation. Therefore, Mode 1 can provide wider bandwidth at certain efficiency level than Mode 2.

For the higher frequencies, the situation is more complicated since the number of modes is larger and it is difficult to excite only certain modes for the needed frequency bands. However, at higher frequencies, the correlation between different antennas is in general lower than in the lower frequencies, and therefore achieving good MIMO performance is not as difficult as in the low band.

B. Antenna Cluster Concept

Antenna cluster concept, first presented in [16], utilizes multiple mutually coupled elements fed with complex weighted signals collaboratively as one antenna. In previously published designs [17], [22], this technique has been used to improve matching and coupling across wide frequency bands for clusters formed from closely spaced self-resonant antenna elements. In this letter, we utilize the CMA together with the antenna cluster technique. Using antenna clusters, we can place multiple capacitive coupling elements close to one or several of the current distribution minima of the characteristic modes to benefit from the otherwise detrimental coupling between the elements and excite the modes more efficiently than with just one element.

The matching efficiency of an antenna cluster can be calculated from the scattering parameters as

$$\eta_{\text{match}} = \frac{\mathbf{a}^{\text{H}}\mathbf{D}\mathbf{a}}{\mathbf{a}^{\text{H}}\mathbf{a}} \tag{1}$$

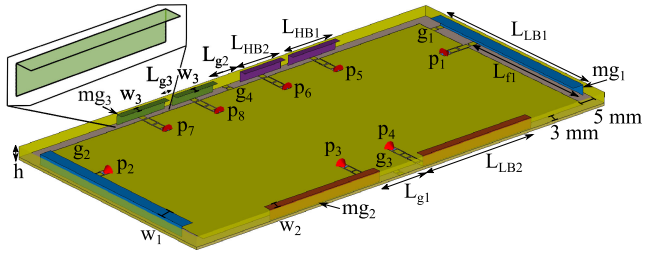

Fig. 2. Proposed antenna structure with a close-up of one of the inverted-L antenna elements. Elements forming one antenna cluster are marked with the same color.

where the radiation matrix $\mathbf{D}$ is defined as

$$\mathbf{D} = \mathbf{I} - \hat{\mathbf{S}}^{\text{H}}\hat{\mathbf{S}}. \tag{2}$$

$\mathbf{a}$ is the complex excitation vector, and $\hat{\mathbf{S}}$ is the scattering matrix where only the columns corresponding to the elements forming the active cluster are used to take into account the coupling to the ports of other antenna clusters [22]. The maximum obtainable efficiency is the largest eigenvalue of $\mathbf{D}$, and the excitation vector $\mathbf{a}$ is the eigenvector corresponding to the largest eigenvalue

$$\eta_{\text{match,max}} = \max\left\{\text{eig}(\mathbf{D})\right\}. \tag{3}$$

To take into account the full antenna structure, i.e., all losses and other factors, the radiation matrix can also be calculated from the far-field patterns of the antennas [23]. Then, the elements of $\mathbf{D}$ are defined as

$$D_{ij} = \iint_{4\pi} F_i \cdot F_j^* \, d\Omega \tag{4}$$

where F_i is the radiation pattern of the ith feed port normalized so that D_{ii} gives the total efficiency of the ith antenna [22]. In this letter, (2) is used for the matching network design and (4) for calculating the total efficiency from the far-field patterns.

III. Antenna and Matching Network Design

A. Antenna Structure

The starting point for the antenna structure is the same as the one used for the CMA in Section II-A. A 0.8 mm thick Rogers RO4003C ($\varepsilon_r = 3.38$, $\tan\delta = 0.0021$) substrate is added for practical realization. The excitation elements are inverted-L-shaped coupling elements placed between the ground plane and the metal rim. The vertical parts of the elements extend to the upper edge of the rim and the bent part to the edge of the ground plane in the horizontal plane. The shape of the antenna element is shown in Fig. 2. The initial positions of the elements are chosen based on the results of the CMA from Section II-A.

To excite the two orthogonal low-band modes shown in Fig. 1, elements are placed near the minima of both current distributions. For Mode 1, the elements forming one antenna cluster are placed at the opposite short edges of the ground plane, marked with feed ports p_1 and p_2. In addition, for improved performance, grounding elements between the antenna element and the ground plane are used. These are marked with g_1 and g_2. Mode 2 is excited with a cluster of elements that are placed on

the long edge of the ground plane (p_3 and p_4) leaving space for the high-band elements on the other side.

The high-band elements are placed on the other long edge. In addition to the antenna elements, grounding elements between the metal rim and the ground plane in the middle of the long edge are also used (g_3 and g_4). The four elements can form the two element antenna clusters in three different combinations. All options are studied, but the final structure uses the option shown in Fig. 2 (p_5–p_8).

B. Matching Network Optimization

The used antenna elements are nonresonant, and matching networks are needed with the antenna elements. Because commercially available matching circuit tools optimize only reflection and coupling losses for traditional antenna systems, these cannot be used for designing matching networks for antenna clusters.

An optimization tool based on genetic algorithm in MATLAB [24] is developed to find the matching circuit topologies and component values. Genetic algorithm is well suited for matching circuit design because it can be used for integer optimization to find the optimal discrete component values from a limited set of models of realistic components and it can utilize parallel computing to speed up the optimization process.

The fitness function to be minimized is formed from the matching efficiencies of the antenna clusters calculated from the *S*-parameter model of the antenna and (2) and (3). To find the solution with optimal performance, a single number that takes into account the minimum and average efficiencies in all frequency bands is calculated as

$$\begin{aligned} \mathrm{FN} = A \sum_n a_n \left(g_{\mathrm{min},n} - \eta_{\mathrm{min},n}\right) \\ + B \sum_n b_n \left(g_{\mathrm{mean},n} - \eta_{\mathrm{mean},n}\right) \end{aligned} \tag{5}$$

where $g_{\mathrm{min},n}$ and $g_{\mathrm{mean},n}$ are set goals for each frequency band and $\eta_{\mathrm{min},n}$ and $\eta_{\mathrm{mean},n}$ are the minimum and average efficiencies for the corresponding bands. A, B, a_n, and b_n are weighting coefficients for each frequency band. The coefficients are chosen such that the value is largest for the band that differs most from the set goal. By tuning the weighting coefficients properly, it is possible to get a desired performance level for all frequency bands.

C. Results

For the final design, the dimensions and exact placement of the antenna elements and the locations of the feedlines and the grounding elements are optimized together with matching circuits. To limit the complexity of the matching circuits, a symmetry plane through the middle of the long edges of the ground plane is applied. 3–4 matching components are used for each antenna element. Based on the CMA results of Section II-A, the low-band cluster 1 is optimized for 700–960 MHz band and cluster 2 for the narrower 824–960 MHz band. The high-band clusters are optimized for 1.7–2.7 and 3.4–3.8 GHz bands. The proposed antenna structure is shown in Fig. 2, and the dimensions in Table I. Antenna elements forming one antenna cluster are marked with one color. Fig. 3 shows the matching circuit topologies and the component values.

TABLE I
DIMENSIONS OF THE PROPOSED ANTENNA

Parameter	L_{LB1}	L_{LB2}	L_{HB1}	L_{HB2}	L_{g1}	L_{g2}	L_{g3}
Value (mm)	60	40	17.5	15	16	10	2.75
Parameter	w_1	w_2	w_3	h	mg_1	mg_2	mg_3
Value (mm)	3.75	2.5	2	4	1.25	0.5	1

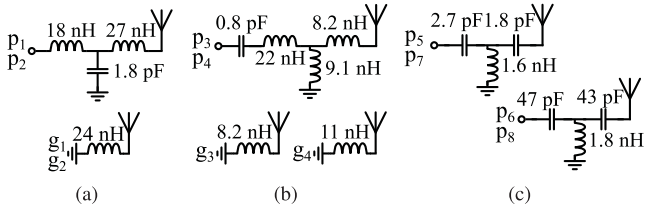

Fig. 3. Realized matching circuits (a) low-band cluster 1, (b) low-band cluster 2 and metal rim groundings, and (c) high-band clusters.

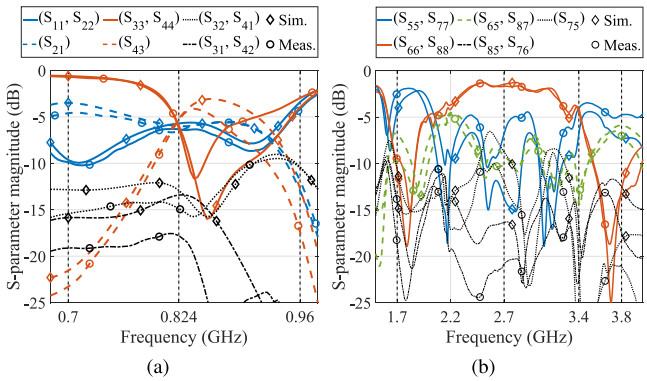

Fig. 4. Simulated and measured *S*-parameters for (a) low band and (b) high band.

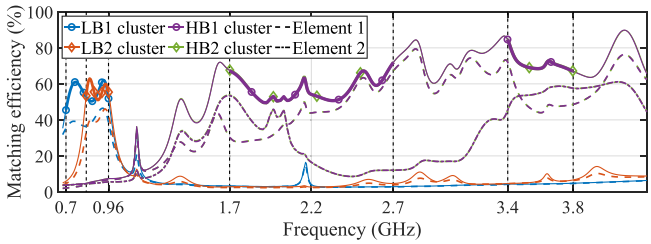

Fig. 5. Simulated matching efficiencies.

Fig. 4 shows the resulting *S*-parameters, and Fig. 5 the corresponding matching efficiencies of the antenna clusters and the individual elements. The low-band results show that there is high coupling between the elements in both clusters, but good isolation between the different clusters. Due to the cluster technique, this coupling is beneficial for the operation.

Better than 50% matching efficiency is achieved in practically the whole operation band. The low-band and high-band

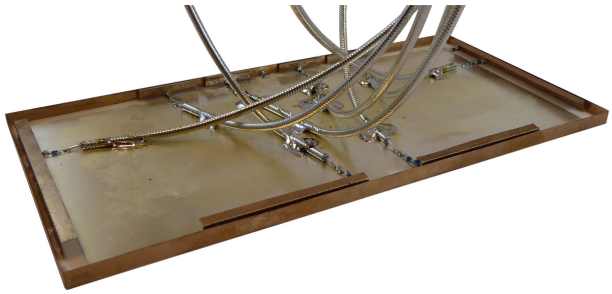

Fig. 6. Manufactured prototype.

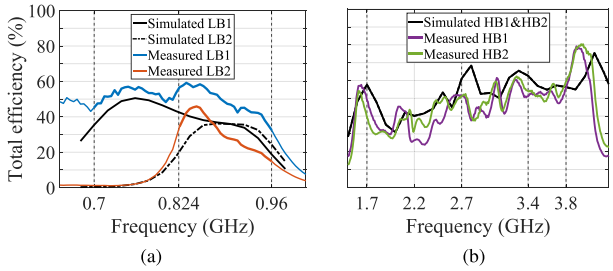

Fig. 7. Simulated and measured total efficiencies for (a) low band and (b) high band.

results show two ways of utilizing the antenna cluster technique: combining operation of two elements with similar frequency response (low band) or two elements with different response (high band).

IV. Prototype and Results

A prototype is manufactured and measured with MVG StarLab 6 GHz antenna measurement system. The prototype with the attached feed cables is shown in Fig. 6. The far-field patterns of each element are measured individually with other ports terminated with 50 Ω loads, and (3) and (4) are used to evaluate the antenna cluster performance. The simulated and measured total efficiencies of the antenna clusters are shown in Fig. 7. For the low-band clusters, the amplitudes of the feeds are equal and the phase difference for ports 1 and 2 is 180° and 0° for ports 3 and 4. For the high-band clusters, the complex feeding weights of the clusters are changed throughout the band to obtain the optimum performance.

The MIMO performance is evaluated by calculating the ergodic capacity [25]. The capacity is calculated with commonly used values of 20 dB SNR and 10^4 Rayleigh fading channel realizations. The simulated and measured envelope correlation coefficients (ECC) and MIMO capacities are shown in Fig. 8 and Fig. 9, respectively.

In general, there is a good agreement between the simulation and measurement results. Over 40% total efficiency is achieved in the 700–940 MHz band, and over 20% in the 820–940 MHz band. The whole band from 1.56 to 4 GHz is covered with 25%–80% efficiency. A comparison of the proposed design and some recently published two-element MIMO antenna designs is given in Table II. When taking into account the covered frequency

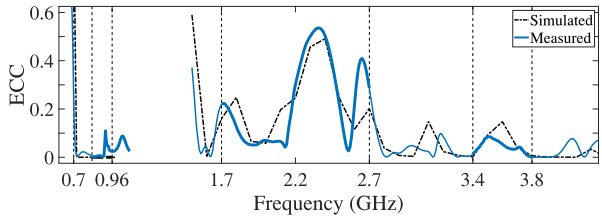

Fig. 8. Simulated and measured ECC.

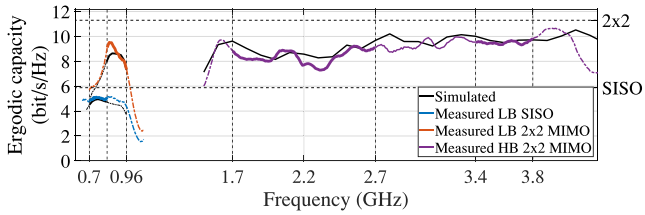

Fig. 9. Simulated and measured MIMO capacity. The ideal capacities of 2 × 2 MIMO and single-input–single-output (SISO) correspond to cases with 100% efficient antennas having zero correlation.

TABLE II
Comparison of the Proposed Design With Recent Unbroken Metal Rim MIMO Antenna Designs

Antenna	Clearance (mm) short/long edge	Frequency bands (GHz)	Efficiency (%)
Prop.	**5/3**	**LB: 0.7–0.96/0.824–0.96** **HB: 1.56–4**	**32–59/15–46** **25–80**
[8]	4/4	LB: 0.742–1/0.863–0.956	40–78/40–65
[10]	2/4	LB: 0.86–0.99	39–58/26–52
[12]	8/2	LB: 0.824–0.96 HB: 1.7–2.7	40–48 59–72
[14]	10/2	LB: 0.824–0.96 HB: 1.7–2.7	31–38 42–69

bands, required ground clearances, and the achieved efficiencies, the proposed design shows competitive performance. The maximum ECC is about 0.54, and it is below 0.2 in most of the operation band, meaning that the effect of correlation on the capacity is small [25]. The achieved capacity for the single antenna in the 700 MHz band is about 5 bit/s/Hz, which corresponds to 85% of the ideal, and the 2 × 2 MIMO capacity is 7.3–9.8 bit/s/Hz in the whole operation band, which is 65%–87% of the ideal value.

V. Conclusion

A MIMO antenna system for a mobile device with unbroken metal rim has been presented in this letter. The proposed design demonstrates how antenna elements with matching circuits can be used with the antenna cluster technique to effectively excite the modes of the metal rim. By utilizing the CMA and the different modes of the metal rim, MIMO operation both in the low and high bands is achieved. The proposed antennas can cover two wide frequency ranges in 700–960 MHz and 1.56–4 GHz bands. Results are confirmed with manufactured and measured prototype, and good performance is achieved despite the small ground clearances and small height of the antenna structure.

REFERENCES

[1] Q. Guo, R. Mittra, F. Lei, Z. Li, J. Ju, and J. Byun, "Interaction between internal antenna and external antenna of mobile phone and hand effect," *IEEE Trans. Antennas Propag.*, vol. 61, no. 2, pp. 862–870, Feb. 2013.

[2] H. Chen and A. Zhao, "LTE antenna design for mobile phone with metal frame," *IEEE Antennas Wireless Propag. Lett.*, vol. 15, pp. 1462–1465, 2016.

[3] Y. Liu, Y. Zhou, G. Liu, and S. Gong, "Heptaband inverted-F antenna for metal-rimmed mobile phone applications," *IEEE Antennas Wireless Propag. Lett.*, vol. 15, pp. 996–999, 2016.

[4] M. Stanley, Y. Huang, H. Wang, H. Zhou, Z. Tian, and Q. Xu, "A novel reconfigurable metal rim integrated open slot antenna for octa-band smartphone applications," *IEEE Trans. Antennas Propag.*, vol. 65, no. 7, pp. 3352–3363, Jul. 2017.

[5] J. Kurvinen, A. Lehtovuori, J. Mai, C. Wang, and V. Viikari, "Metal-covered handset with LTE MIMO, Wi-Fi MIMO, and GPS antennas," *Prog. Electromagn. Res. C*, vol. 80, pp. 89–101, 2018.

[6] Y. Zhang, S. Yang, Y. Ban, Y. Qiang, J. Guo, and Z. Yu, "Four-feed reconfigurable MIMO antenna for metal-frame smartphone applications," *Microw., Antennas Propag.*, vol. 12, no. 9, pp. 1477–1482, 2018.

[7] Y. L. Ban, Y. F. Qiang, Z. Chen, K. Kang, and J. H. Guo, "A dual-loop antenna design for hepta-band WWAN/LTE metal-rimmed smartphone applications," *IEEE Trans. Antennas Propag.*, vol. 63, no. 1, pp. 48–58, Jan. 2015.

[8] C. Deng, Z. Feng, and S. V. Hum, "MIMO mobile handset antenna merging characteristic modes for increased bandwidth," *IEEE Trans. Antennas Propag.*, vol. 64, no. 7, pp. 2660–2667, Jul. 2016.

[9] Y. Yan, Y. Ban, G. Wu, and C. Sim, "Dual-loop antenna with band-stop matching circuit for WWAN/LTE full metal-rimmed smartphone application," *Microw., Antennas Propag.*, vol. 10, no. 15, pp. 1715–1720, 2016.

[10] L. Qu, J. Jeon, D. Park, and H. Kim, "Antenna design based on quasi-degenerate characteristic modes of unbroken metal rim," *Microw., Antennas Propag.*, vol. 11, no. 15, pp. 2168–2173, 2017.

[11] H. Zhang, Y. Ban, Y. Qiang, J. Guo, and Z. Yu, "Reconfigurable loop antenna with two parasitic grounded strips for WWAN/LTE unbroken-metal-rimmed smartphones," *IEEE Access*, vol. 5, pp. 4853–4858, 2017.

[12] Z. Xu, Y. Sun, Q. Zhou, Y. Ban, Y. Li, and S. S. Ang, "Reconfigurable MIMO antenna for integrated-metal-rimmed smartphone applications," *IEEE Access*, vol. 5, pp. 21 223–21 228, 2017.

[13] Z. Xu, Q. Zhou, Y. Ban, and S. S. Ang, "Hepta-band coupled-fed loop antenna for LTE/WWAN unbroken metal-rimmed smartphone applications," *IEEE Antennas Wireless Propag. Lett.*, vol. 17, no. 2, pp. 311–314, Feb. 2018.

[14] L. Zhang, Y. Ban, C. Sim, J. Guo, and Z. Yu, "Parallel dual-loop antenna for WWAN/LTE metal-rimmed smartphone," *IEEE Trans. Antennas Propag.*, vol. 66, no. 3, pp. 1217–1226, Mar. 2018.

[15] C. Deng, Z. Xu, A. Ren, and S. V. Hum, "TCM-based bezel antenna design with small ground clearance for mobile terminals," *IEEE Trans. Antennas Propag.*, vol. 67, no. 2, pp. 745–754, Feb. 2019.

[16] J.-M. Hannula, J. Holopainen, and V. Viikari, "Concept for frequency-reconfigurable antenna based on distributed transceivers," *IEEE Antennas Wireless Propag. Lett.*, vol. 16, pp. 764–767, 2017.

[17] J.-M. Hannula, T. Saarinen, J. Holopainen, and V. Viikari, "Frequency reconfigurable multiband handset antenna based on a multichannel transceiver," *IEEE Trans. Antennas Propag.*, vol. 65, no. 9, pp. 4452–4460, Sep. 2017.

[18] R. Harrington and J. Mautz, "Theory of characteristic modes for conducting bodies," *IEEE Trans. Antennas Propag.*, vol. AP-19, no. 5, pp. 622–628, Sep. 1971.

[19] R. Martens, E. Safin, and D. Manteuffel, "Inductive and capacitive excitation of the characteristic modes of small terminals," in *Proc. Loughborough Antennas Propag. Conf.*, Nov. 2011, pp. 1–4.

[20] R. Martens and D. Manteuffel, "Systematic design method of a mobile multiple antenna system using the theory of characteristic modes," *Microw., Antennas Propag.*, vol. 8, no. 12, pp. 887–893, Sep. 2014.

[21] H. Li, Y. Tan, B. K. Lau, Z. Ying, and S. He, "Characteristic mode based tradeoff analysis of antenna-chassis interactions for multiple antenna terminals," *IEEE Trans. Antennas Propag.*, vol. 60, no. 2, pp. 490–502, Feb. 2012.

[22] J.-M. Hannula, T. O. Saarinen, A. Lehtovuori, J. Holopainen, and V. Viikari, "Tunable eight-element MIMO antenna based on the antenna cluster concept," *Microw., Antennas Propag.*, Feb. 2019. [Online]. Available: https://digital-library.theiet.org/content/journals/10.1049/ietmap.2018.5742

[23] C. Volmer, M. Sengul, J. Weber, R. Stephan, and M. A. Hein, "Broadband decoupling and matching of a superdirective two-port antenna array," *IEEE Antennas Wireless Propag. Lett.*, vol. 7, pp. 613–616, 2008.

[24] MathWorks Inc., "Genetic algorithm: Find global minima for highly nonlinear problems," Natick, MA, USA, 2018. Accessed: Oct. 23, 2018. [Online]. Available: https://se.mathworks.com/discovery/genetic-algorithm.html

[25] R. Tian, B. K. Lau, and Z. Ying, "Multiplexing efficiency of MIMO antennas," *IEEE Antennas Wireless Propag. Lett.*, vol. 10, pp. 183–186, 2011.